Published in final edited form as:

ACS Nano. 2015 August 25; 9(8): 8231–8238. doi:10.1021/acsnano.5b02595.

Anomalously Fast Diffusion of Targeted Carbon Nanotubes in Cellular Spheroids

Yichun Wang[†,‖], **Joong Hwan Bahng**[†,‖], **Quantong Che**[‡], **Jishu Han**[‡], **Nicholas A. Kotov**[*,†,‡,§,‖]

[†] Department of Biomedical Engineering, University of Michigan, 3074 H.H. Dow Building, 2300 Hayward Street, Ann Arbor, Michigan 48109, United States

[‡] Department of Chemical Engineering, University of Michigan, 3074 H.H. Dow Building, 2300 Hayward Street, Ann Arbor, Michigan 48109, United States

[§] Department of Material Science & Engineering, University of Michigan, 3074 H.H. Dow Building, 2300 Hayward Street, Ann Arbor, Michigan 48109, United States

[‖] Biointerfaces Institute, University of Michigan, North Campus Research Complex, 2800 Plymouth Road, Ann Arbor, Michigan 48109, United States

Abstract

Understanding transport of carbon nanotubes (CNTs) and other nanocarriers within tissues is essential for biomedical imaging and drug delivery using these carriers. Compared to traditional cell cultures in animal studies, three-dimensional tissue replicas approach the complexity of the actual organs and enable high temporal and spatial resolution of the carrier permeation. We investigated diffusional transport of CNTs in highly uniform spheroids of hepatocellular carcinoma and found that apparent diffusion coefficients of CNTs in these tissue replicas are anomalously high and comparable to diffusion rates of similarly charged molecules with molecular weights 10000× lower. Moreover, diffusivity of CNTs in tissues is enhanced after functionalization with transforming growth factor β1. This unexpected trend contradicts predictions of the Stokes–Einstein equation and previously obtained empirical dependences of diffusivity on molecular mass for permeants in gas, liquid, solid or gel. It is attributed to the planar diffusion (gliding) of CNTs along cellular membranes reducing effective dimensionality of diffusional space. These findings indicate that nanotubes and potentially similar nanostructures are capable of fast and deep permeation into the tissue, which is often difficult to realize with anticancer agents.

Graphical Abstract

[*]Address correspondence to kotov@umich.edu.

Conflict of Interest: The authors declare no competing financial interest.

Supporting Information Available: Quantitative analysis of experimental/effective diffusion coefficients; calculation of theoretical and apparent diffusion coefficients; additional methods and figures. The Supporting Information is available free of charge on the ACS Publications website at DOI: 10.1021/acsnano.5b02595.

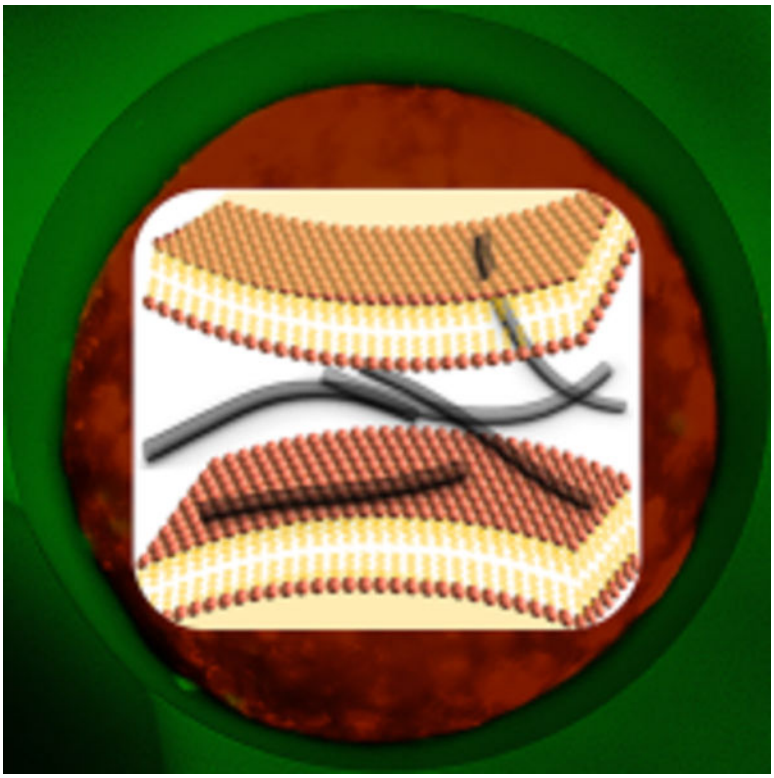

Keywords

nanoscale drug carriers; carbon nanotubes; diffusion; drug delivery; three-dimensional cell culture; ICC scaffolds

Carbon nanotubes (CNTs) have emerged as promising drug delivery and imaging vehicles for treatment of cancer and other diseases.[1–4] Their unique optical, electronic, and biological properties enable more efficient methods of therapy, more accurate diagnostics, and potentially reduced side effects than some other drug carriers (Supporting Information). Realization of this promise, however, is impeded, among other factors, by poor understanding of their transport in tissues. The knowledge of how CNTs permeate through the tumor mass is particularly essential when targeting dormant cancer cells located deep within tumors responsible for the cancer recurrences.[5] Despite that, the basic characteristics of their transport in tissues and its governing mechanisms are largely unknown. The problems with determination of, for instance, diffusion coefficient, D, of CNTs in tissues is associated with fundamental difficulties of tracking nanoscale carriers in highly scattering media.[6] CNT permeation profiles obtained by dissection of animal organs are difficult to analyze from the perspective of transport mechanisms because of limited quantity of time points, natural variability of animals, and blood circulation.[7–9] Addressing primarily the toxicological issues of CNTs,[10] the current biodistribution data in animals were obtained with widely different protocols from various tumor models, therapeutic modalities, administration routes, nanotube doses, and quantification methods (Supporting Information). They are also expensive and laborious. Evaluation of CNT transport in

traditional two-dimensional (2D) cell cultures is technically and economically accessible but they lack biological sophistication of tissues.[11–13] Three-dimensional (3D) cell cultures are convenient research alternatives to 2D cell cultures and animals because they represent the intermediate level of complexity of the biological models *in vitro*. 3D cell cultures may serve as new tools for more accurate and effective assessment for transport of CNTs and other drug carriers in organs/tissues complementing the use of other models. The ethical aspects of the sacrificing large number of animals for statistical purposes must be considered as well.

In this work, we utilized 3D cell cultures in inverted colloidal crystal (ICC) scaffolds[14] to investigate CNT permeation through model tissue of hepatocellular carcinoma based on HepG2 cell line (see the Methods and Figure S1, Supporting Information). ICC scaffolds with uniform porous structure (Figure 1) facilitate formation of nearly perfectly monodispersed spheroids with tissue-like features.[14]

To observe CNTs using standard confocal microscopes inside the spheroids, we labeled them with the standard luminescent tag FITC. Transforming growth factor β1 (TGFβ1) was chosen as the targeting ligand because TGFβ receptors are present in HepG2 cells[15,16] and up-regulated in many cancers. The nanotubes without targeting ligand are referred to as CNT-FITC, while the ones carrying both TGFβ1 and FITC are referred to as CNT-TGFβ1-FITC. The total load of the TGFβ1 per CNT was 1.13×10^{-17} g, which amounts to 2.6 ± 0.3 molecules of the targeting ligands. The average molecular weight (M_r) of CNT-TGFβ1-FITC was 6.84×10^6 Da. It can be compared to $M_r = 6.79 \times 10^6$ Da of the CNT-FITC that is $5.83 \pm 0.74 \times 10^4$ Da lighter (see the Methods and Figure S2, Supporting Information). The electrokinetic ζ-potentials (ζ) of CNT-TGFβ1-FITC and CNT-FITC were −8.4 ± 0.306 and −0.01 ± 0.001 mV, respectively (Table 1).

RESULTS AND DISCUSSION

To visualize green-fluorescing CNT-FITC and CNT-TGFβ1-FITC on the background of tissue spheroids, HepG2 cells were labeled by CellTracker CMRA (Invitrogen, US) with orange-red luminescence. In some cases, HepG2 cells in spheroids were stained by CellTracker Red CMTPX dye or 5-chloromethylfluorescein diacetate (CMFDA) (Life Technologies, US) with red and green luminescence, respectively. Z-stack images of multiple spheroids (Figure 2g,h and Figures S4–S9, Supporting Information) were captured at 20, 40, 60, 80, 100, and 120 min after addition of permeants to the cell culture. Concentration profiles inside the spheroids were derived from the fluorescent intensity of the permeants (Figure 2c–f). Apparent diffusion coefficients, D_a, reflecting the experimentally observable rate of their transport were obtained for FITC, rhodamine B (RhB), TGFβ1, CNT-FITC, and CNT-TGFβ1-FITC by fitting the progression of experimental diffusion profiles with the Second Fick's law (Table 1) using our own code (Supporting Information).

The values D_a for FITC and RhB indicate that diffusion of these small molecules in cellular spheroids grown in ICC scaffolds are similar to those observed previously in solid tissues (Supporting Information);[17] these data provided us useful benchmarks and validated our methods.

As anticipated from the previous studies,[3,18] diffusivity of the small luminescent molecules in tissue model is strongly dependent on charge, with $D_a = \left(5.9 \pm 0.3\right) \times 10^{-13}$ m^2/s for RhB being considerably higher than $D_a = \left(1.6 \pm 0.3\right) \times 10^{-14}$ m^2/s for FITC. The positive charge of RhB is facilitated by electrostatic attraction to negatively charged cellular membranes. We noticed that $D_a = \left(0.9 \pm 0.3\right) \times 10^{-14}$ m^2/s of CNT-FITC is comparable to the diffusion coefficient of free FITC. Note that the average molecular mass $M_r = 6.79 \times 10^6$ Da of CNT-FITC is 1.7×10^4 Da larger than that of FITC with $M_r = 389.4$ Da. The startling closeness of diffusivity for these two species contradicts known trends for diffusivity of permeants in gas, liquid, solid or gel. As such, diffusivity CNT-FITC predicted by Einstein–Stokes diffusion equation for rodlike particles is lower by almost 2 orders of magnitude relative to experimental values (Table 1 and Figure S16, Supporting Information). Although approximate, the Einstein–Stokes diffusion equation correctly predicts the increased friction coefficients between permeants and fluid for rod shaped particles and typically yields a reasonably good match with experimental values. Note also that both FITC and CNT-FITC have negative charge, and “acceleration” of nanotube transport cannot be attributed solely to favorable electrostatic interactions with cellular membranes. Furthermore, at $(1.5 \pm 0.2) \times 10^{-13}$ m^2/s, the D_a of CNT-TGFβ1-FITC markedly exceeds the diffusion coefficients of both CNT-FITC and FITC, despite even greater $M_r = 6.84 \times 10^6$ Da. One should also mention that diffusion of CNTs in blood, lymph, and bile[19] with D_a equal to $(0.59 \pm 0.18) \times 10^{-14}$ m^2/s, $(1.45 \pm 0.65) \times 10^{-14}$ m^2/s, and $(0.9 \pm 0.2) \times 10^{-14}$ m^2/s, respectively, is considerably slower,[19] which is also counterintuitive considering that these tissues are liquid. Experimental observations of CNT transport in dense bacterial biofilms[20] and glomerular membranes[21] confirm that nanotube transports in dense biological media can be described as paradoxical, with several possible causes.

The unexpectedly high diffusion coefficients of CNTs in dense tissues were puzzling, and we decided to verify the permeation of CNT-TGFβ1-FITC through the 3D tissue models using microscopy techniques to avoid potential artifacts associated, for instance, with the slow detachment of FITC from nanotubes. After exposure of spheroids to CNTs-TGFβ1-FITC for 20 min, the nanotubes were found to be imbedded in the cellular mass (Figure 3a–c, Methods, and Supporting Information). The comparable scanning electron microscopy images of the spheroids prior to exposure to nanotube dispersion can be found in Figure 1b. To verify permeation of CNTs into the central part of the spheroid, we also carried out histological sectioning of the ICC scaffolds. CNTs can be found in SEM images of the slices of the spheroids obtained at the middle focal plane ~38 μm from the spheroid’s surface (Figure 3e,f), which agrees with the permeation profiles in Figure 2g. The collected microscopy and calculation data in Figures 1 and 2 and Table 1 indicate that biochemical interaction of CNTs with the tissue model strongly alters their transport compared to purely Brownian diffusion.[22,23]

Let us now consider possible pathways of CNT transport in the cellular spheroids. CNTs can permeate through the interstitial space and across/along the cell membranes.[7,24] In addition to the Brownian diffusion, this transport process is also influenced by the

interaction of CNTs with extracellular matrix (ECM) and living cells, which is expected to affect their overall mobility in tissues.[25,26] The transport processes at the cellular interface include adsorption to the cellular membrane, surface diffusion, desorption from the cellular membrane, endocytosis, and exocytosis (Scheme S1, Supporting Information). Cumulatively, the transport of CNTs in tissue can be described by a differential equation

$$\frac{\partial C_{ex}}{\partial t} = \nabla(D_{ex}\nabla C_{ex} - uC_{ex}) - R \quad (1)$$

where the concentration of CNT in interstitial/extracellular space is C_{ex} and u is the comvection coefficient.[27] D_{ex} is the diffusion coefficient in the extracellular spaces, approximated as homogeneous aqueous media. [11,28] Biological interactions of the CNTs with the ECM and cellular membrane are represented by the reaction term R.[29] Diffusion conditions specific for tissue model allow us to simplify eq 1. First, ICC scaffolds prevent macroscopic fluid flow and, thus, convection term uC_{ex} can be eliminated. Second, within the 120 min of our experiment, exocytosis component of the term R of CNT has minimal effect on transport process as reported by Jin *et al.*[11] The remaining components of R for CNT-FITC and CNT-TGFβ1-FITC can be evaluated in 2D cell culture.

To quantify the endocytotic component of R, HepG2 cells were incubated with CNTs-FTC and CNTs-TGFβ1-FITC at both 4 and 37 °C for 1 h. Statistically identical small amounts of CNTs-FIC and CNTs-TGFβ1-FTTC were internalized by cells for both experimental conditions (Figure 4). Since at 4 °C endocytosis is arrested, the endocytotic component of R for these permeants can be neglected for experimental conditions described in this study that include the liver tissue model and period of CNT diffusion experiment.

Adsorption to, surface diffusion on, and desorption from the cellular membranes of CNTs make, therefore, the primary contributions to R Equation 1 should be rewritten then as a system of differential equations

$$\begin{cases} \frac{\partial C_{ex}}{\partial t} + \frac{\partial C_{mem}}{\partial t} = \nabla(D_{ex}\nabla C_{ex}) + \nabla'(D_{mem}\nabla' C_{mem}) - (k_a C_{ex} - k_d C_{mem}) \\ \frac{\partial C_{ex}}{\partial t} = \nabla(D_{ex}\nabla C_{ex}) \\ \frac{\partial C_{mem}}{\partial t} = \nabla'(D_{mem}\nabla' C_{mem}) \end{cases} \quad (2)\ (3)\ (4)$$

where C_{mem} is the concentration on the cell membrane, k_a and k_d are the first-order rate constants for adsorption and desorption of CNTs on membranes, ∇' is the Laplace operator for 2D diffusion, and D_{mem} is the coefficient for the diffusion along the cell membrane. Since binding/unbinding processes are reversible and fast with characteristic times of milliseconds,[30] we can add another equation to this system

$$C_{mem}/C_{ex} = k_a/k_a = K$$

(5)

where K is the equilibrium constant ($K > 0$) for CNT two-phases distribution between the interstitial space and membrane surface.

Note that ∇ and ∇' have different systems of coordinates that are "natural" for 3D bulk and 2D surface diffusion processes. It is possible to transform ∇' into Cartesian coordinates but it will require additional boundary conditions and separate geometrical description of the membrane surface. Note also that D_{mem} is logarithmically dependent on the membrane curvature and the size of the permeant.[31] Even after some simplification including eq 5, this system of differential equations is difficult for an analytical solution. It can be solved, however, by using Monte Carlo simulations. Similar problem was encountered in the past for diffusion for small molecules in porous solids.[32] On the basis of the diffusion pathways for combined 2D (surface-confined) and 3D (bulk) diffusion, an apparent diffusion coefficient can be calculated as (Supporting Information)

$$D_a = \frac{D_{ex}\phi}{\tau_{ex}} + \frac{D_{mem}}{\tau_{mem}} a_v K \tag{6}$$

where τ_{ex} and τ_{mem} denote the void and surface tortuosities, ϕ is volume fraction of voids in cellular spheroids, and a_v is the ratio of the volume of cell membrane to the volume of the interstitial spaces on the cellular spheroid voids. These parameters can be estimated using experimental results for hepatocytes, cellular spheroids, and tumors: $\tau_{ex} = \tau_{mam} = 0.6$, $\phi = 60\%$, and $a_v = 0.012$ (Supporting information). D_{mem} can be treated as a surface-averaged constant and was calculated for diffusion coefficient of membrane proteins to be $(2.3 \pm 0.7) \times 10^{-12}$ m^2/s.[31] Since lymph is essentially an interstitial fluid, we take the diffusion coefficient of CNTs in lymph as D_{ex}, *i.e.*, $(1.45 \pm 0.65) \times 10^{-14}$ m^2/s.[19] D_a from eq 6 for CNT-FIC and CNT-TGFβ1-FITC is equal to $(0.9 \pm 0.3) \times 10^{-14}$ m^2/s and $(1.5 \pm 0.2) \times 10^{-13}$ m^2/s (Table 1). Therefore, one can calculate the equilibrium constants $K_{CNT-FITC} = 0$ and $K_{CNT-TGF\beta1-FITC} = 2.95$ for CNT-FITC, CNT-TGFβ1-FITC respectively (Supporting Information). These values are in agreement with each other, as one would expect that the affinity of surface ligands to the cells surface increases with addition of TGFβ1 to CNTs. The presence of carboxyl groups on CNT-TGFβ1-FITC is likely to play a role as well because they are less adhesive to cells than the targeting ligand.[33] Given the overall tendency for the CNTs-based permeants to adhere to cell membranes, the negative charges of CNT-TGFβ1-FITC and CNT-FITC (Table 1) are likely to stimulate the lateral 2D diffusion by reducing internalization in the tissue model from HepG2 cells, which allows unbounded CNTs to diffuse further and faster.

Thus anomalously high values of D_a of CNT-TGFβ1-FITC should be attributed to the contribution of the lateral diffusion along the cellular surface to the overall transport.[11,13] Electrostatic repulsion between CNT-TGFβ1-FITC and cellular membrane facilitate the lateral motion akin to gliding. The partial confinement to the surface due to the presence of targeting ligands dramatically accelerates the transport of the permeant, despite the overall

increase in mass, and results in anomalously high diffusivities. Similar transition from 3D to 2D diffusion in tissues is also known for some proteins that roll across the cellular membrane.[11]

CONCLUSIONS

The method described in this work enables accurate and systematic evaluation of the different modes of transport of CNTs and CNT-based drug delivery systems necessary for comprehensive pharmacokinetic models.[34] In the same manner, *in vitro* 3D cell cultures in ICC scaffolds can be easily applied to other molecules/nanoscale carriers and offer possibility for simple comparative studies between different drug carriers in the absence of complicating factors such as pharmacokinetics and metabolism.[35] The developed computational model can be utilized in the design drug delivery systems with optimal diffusion and cellular affinity, ensuring transport deep within the tumor and sufficient accumulation to elicit a therapeutic effect. In future studies, incorporation of the physical and chemical parameters such as fluid flow and shear force into the 3D tissue model should be pursued to provide more detailed insight into the effects of CNT-tissue on transport efficiency. The required numerical data to be incorporated in the set of differential equations describing transport in tissues can be obtained with the help of advanced spectroscopic tools.[36] *In vivo* studies will be desirable to standardize the data obtained from the 3D model for clinical use. Besides drug delivery, the knowledge about the CNT diffusion in the tissues can also be extended toward toxicological studies of free CNTs and nanotube based composites to be used as biomedical implants.[37,38]

METHODS

Fabrication of ICC Scaffolds.

ICC scaffolds were utilized to obtain tumor-like HepG2 spheroids as described in previous work;[14] polyacrylamide hydrogel ICC scaffolds were prepared by utilizing colloidal crystals (CC) as templates. To control the pore size, we used uniform glass beads with diameters of 170 μm. The 3D structure of CC with high connecton can be achieved by annealing at 680 °C for 3 h followed by transfer into ICC geometry high porosity.

Cell Culture.

HepG2 human hepatocellular carcinoma cells (HB-8065) (ATCC, VA) were maintained with Eagle's minimum essential medium (EMEM) supplemented with 10% fetal bovine serum (FBS) and 1% penicillin–streptomycin (ATCC). To form tissue-like cell spheroids, the medium was filtered using a 0.22 μm SteriCup filter assembly (Millipore, USA) and stored at 4 °C for no longer than 2 weeks.

Cellular Spheroids in 3D ICC Scaffolds.

A total of 500000 cells in 25 μL of dense cell suspension (2×10^7 cells/mL) was dropped onto a completely dried hydrogel ICC scaffold using a micropipette, and 975 μL of media was gently added. Total culture volume was maintained at 1000 μL, and half of the media was changed every 2 days. Nearly perfectly monodispersed spheroids were observed after

5 days of culture in high yield (details of cell culture protocol are given in the Supporting Information). Previous data indicate structural features including the development of an ECM membrane coating their surface and abnormal bile canaliculated structures, which replicate solid tumors in cancer tissue.

Preparation of Targeted CNTs with Fluorescence Tags.

CNTs were functionalized by covalent attachment of the targeting ligand, TGFβ1 (Life Technologies). In short, 0.5 mg CNTs with an average diameter of 1.2 nm and a length of 1000 nm (0.5 mg/mL, P3SWNT with 1.0–3.0 atomic % carboxylic acid, Carbon Solutions, Inc.) were dispersed in phosphate-buffered saline (PBS) buffer followed by incubation with 8 mg of 1-ethyl-3-(3-(dimethylamino)-propyl)carbodiimide (EDAC) for 1 min at room temperature, after which samples were immediately vortexed. Next, TGFβ1 5 μg in 50 μL of PBS and FITC (Life Technologies) (2 μg in 20 μL of DMF) were added together, and the resulting mixture was allowed to react for an additional 2 h at 37 °C in a rotator rocker. These samples were then centrifuged at 1300 rpm for 20 min 3× to remove unbound antibodies and excess FITC in Centricon YM-50 tubes (Millipore Corporation, USA), and the resulting CNT-TGFβ1-FITC were suspended in 1 mL of serum-free Eagle's Minimum Essential Medium (EMEM) and used immediately.[39]

Supplementary Material

Refer to Web version on PubMed Central for supplementary material.

Acknowledgment.

This work was supported by the Center for Photonic and Multiscale Nanomaterials (C-PHOM) funded by the National Science Foundation Materials Research Science and Engineering Center program DMR 1120923. We acknowledge support from the NSF under Grant Nos. ECS-0601345, EFRI-BSBA 0938019, CBET 0933384, CBET 0932823, and CBET 1036672. The work is also partially supported by AFOSR MURI 444286-P061716 and NIH 1R21CA121841-01A2. We thank the University of Michigan's EMAL for its assistance with electron microscopy and for the NSF Grant No. DMR-9871177 for funding for the JEOL 2010F analytical electron microscope used in this work. We express our great appreciation to MIL laboratory at the University of Michigan for microscopy and image analysis, to Prof. Jungwoo Lee for help with cellular spheroid culture and scaffold fabrication, and to Mr. Jian Zhu for help with the modification of CNTs.

REFERENCES AND NOTES

1. Feazell RP; Nakayama-Ratchford N; Dai H; Lippard SJ Soluble Single-Walled Carbon Nanotubes as Longboat Delivery Systems for Platinum(Iv) Anticancer Drug Design. J. Am. Chem. Soc. 2007, 129, 8438–8439. [PubMed: 17569542]
2. Liu Z; Chen K; Davis C; Sherlock S; Cao QZ; Chen XY; Dai H Drug Delivery with Carbon Nanotubes for *in Vivo* Cancer Treatment. Cancer Res. 2008, 68, 6652–6660. [PubMed: 18701489]
3. Kotov NA; Winter JO; Clements IP; Jan E; Timko BP; Campidelli S; Pathak S; Mazzatenta A; Lieber CM; Prato M; Bellamkonda RV; Silva GA; Shi Kam NW; Patolsky F; Ballerini L Nanomaterials for neural interfaces, Advanced Materials, 2009, 21 (40), 3970–4004
4. Munzer AM; Michael ZR; Star A Carbon Nanotubes for the Label-Free Detection of Biomarkers. ACS Nano 2013, 7, 7448–7453. [PubMed: 24032561]
5. Minchinton AI; Tannock IF Drug Penetration in Solid Tumours. Nat. Rev. Cancer 2006, 6, 583–592. [PubMed: 16862189]
6. Ferrari M Cancer Nanotechnology: Opportunities and Challenges. Nat. Rev. Cancer 2005, 5, 161–171. [PubMed: 15738981]

7. Singh R; Pantarotto D; Lacerda L; Pastorin G; Klumpp C; Prato M; Bianco A; Kostarelos K Tissue Biodistribution and Blood Clearance Rates of Intravenously Administered Carbon Nanotube Radiotracers. Proc. Natl. Acad. Sci. U. S. A. 2006, 103, 3357–3362. [PubMed: 16492781]
8. Zhang Y; Deng J; Guo F; Li C; Zou Z; Xi W; Tang J; Sun Y; Yang P; Han Z; Li D; Jiang C; Zhang Y Functionalized Single-Walled Carbon Nanotubes Cause Reversible Acute Lung Injury and Induce Fibrosis in Mice. J. Mol. Med. 2013, 91, 117–128. [PubMed: 22878607]
9. Sager TM; Wolfarth MW; Andrew M; Hubbs A; Friend S; Chen TH; Porter DW; Wu N; Yang F; Hamilton RF; Holian A Effect of Multi-Walled Carbon Nanotube Surface Modification on Bioactivity in the C57bl/6 Mouse Model. Nanotoxicology 2014, 8, 317–327. [PubMed: 23432020]
10. Yang K; Liu Z In Vivo Biodistribution, Pharmacokinetics, and Toxicology of Carbon Nanotubes. Curr. Drug Metab 2012, 13, 1057–1067. [PubMed: 22380009]
11. Jin H; Heller DA; Strano MS Single-Particle Tracking of Endocytosis and Exocytosis of Single-Walled Carbon Nanotubes in Nih-3t3 Cells. Nano Lett. 2008, 8, 1577–1585. [PubMed: 18491944]
12. Larson B; Banks P; Sherman H; Rothenberg M Automation of Cell-Based Drug Absorption Assays in 96-Well Format Using Permeable Support Systems. J. Lab. Autom. 2012, 17, 222–232. [PubMed: 22357561]
13. Reuel NF; Dupont A; Thouvenin O; Lamb DC; Strano MS Three-Dimensional Tracking of Carbon Nanotubes within Living Cells. ACS Nano 2012, 6, 5420–5428. [PubMed: 22624495]
14. Lee J; Cuddihy MJ; Cater GM; Kotov NA Engineering Liver Tissue Spheroids with Inverted Colloidal Crystal Scaffolds. Biomaterials 2009, 30, 4687–4694. [PubMed: 19524294]
15. Xu N; Hurtig M; Zhang XY; Ye Q; Nilsson-Ehle P Transforming Growth Factor-Beta Down-Regulates Apolipoprotein M in Hepg2 Cells. Biochim. Biophys. Acta, Mol. Cell Biol. Lipids 2004, 1683, 33–37.
16. Giannelli G; Villa E; Lahn M Transforming Growth Factor-Beta as a Therapeutic Target in Hepatocellular Carcinoma. Cancer Res. 2014, 74, 1890–1894. [PubMed: 24638984]
17. Anissimov YG; Zhao X; Roberts MS; Zvyagin AV Fluorescence Recovery after Photo-Bleaching as a Method to Determine Local Diffusion Coefficient in the Stratum Corneum. Int. J. Pharm. 2012, 435, 93–97. [PubMed: 22326252]
18. Chauhan VP; Jain RK Strategies for Advancing Cancer Nanomedicine. Nat. Mater. 2013, 12, 958–962. [PubMed: 24150413]
19. Judkins J; Lee HH; Tung S; Kim JW Diffusion of Single-Walled Carbon Nanotube under Physiological Conditions. J. Biomed. Nanotechnol 2013, 9, 1065–1070. [PubMed: 23858971]
20. Lawrence JR; Wolfaardt GM; Korber DR Determination of Diffusion Coefficients in Biofilms by Confocal Laser Microscopy. Appl. Environ. Microbiol. 1994, 60, 1166–1173. [PubMed: 16349228]
21. Ruggiero A; Villa CH; Bander E; Rey DA; Bergkvist M; Batt CA; Manova-Todorova K; Deen WM; Scheinberg DA; McDevitt MR Paradoxical Glomerular Filtration of Carbon Nanotubes. Proc. Natl. Acad. Sci. U. S. A. 2010, 107, 12369–12374. [PubMed: 20566862]
22. Fukumori Y; Ichikawa H Nanoparticles for Cancer Therapy and Diagnosis. Adv. Powder Technol. 2006, 17, 1–28.
23. Kanapathipillai M; Brock A; Ingber DE Nanoparticle Targeting of Anti-Cancer Drugs That Alter Intracellular Signaling or Influence the Tumor Microenvironment. Adv. Drug Delivery Rev. 2014, 79–80, 107–118.
24. Nel AE; Madler L; Velegol D; Xia T; Hoek EM; Somasundaran P; Klaessig F; Castranova V; Thompson M Understanding Biophysicochemical Interactions at the Nano-Bio Interface. Nat. Mater. 2009, 8, 543–557. [PubMed: 19525947]
25. Tasis D; Tagmatarchis N; Bianco A; Prato M Chemistry of Carbon Nanotubes. Chem. Rev. 2006, 106, 1105–1136. [PubMed: 16522018]
26. Battigelli A; Menard-Moyon C; Da Ros T; Prato M; Bianco A Endowing Carbon Nanotubes with Biological and Biomedical Properties by Chemical Modifications. Adv. Drug Delivery Rev. 2013, 65, 1899–1920.
27. Liu C; Krishnan J; Stebbing J; Xu XY Use of Mathematical Models to Understand Anticancer Drug Delivery and Its Effect on Solid Tumors. Pharmacogenomics 2011, 12, 1337–1348. [PubMed: 21919608]

28. Verma A; Uzun O; Hu Y; Han HS; Watson N; Chen S; Irvine DJ; Stellacci F; Hu Y Surface-Structure-Regulated Cell-Membrane Penetration by Monolayer-Protected Nanoparticles. Nat. Mater. 2008, 7, 588–595. [PubMed: 18500347]

29. Guo C; Al-Jamal K; Ali-Boucetta H; Kostarelos K Cell Biology of Carbon Nanotubes. Adv. Carbon Nanomater. 2012, 343–368.

30. Liu C; Krishnan; Xu XY Towards an Integrated Systems-Based Modelling Framework for Drug Transport and Its Effect on Tumour Cells. J. Biol. Eng. 2014, 8, 3. [PubMed: 24764492]

31. Domanov YA; Aimon S; Toombes GE; Renner M; Quemeneur F; Triller A; Turner MS; Bassereau P Mobility in Geometrically Confined Membranes. Proc. Natl. Acad. Sci. U. S. A. 2011, 108, 12605–12610. [PubMed: 21768336]

32. Zalc Jeffrey M.; Reyes SC; Iglesia E Monte-Carlo Simulations of Surface and Gas Phase Diffusion in Complex Porous Structures. Chem. Eng. Sci. 2003, 58, 4605–4617.

33. Lee JH; Lee JW; Khang G; Lee HB Cell Behavior on Polymer Surfaces with Different Functional Groups. Sci. Technol. Polym. Adv. Mater. 1998, 535–545.

34. Thurber GM; Weissleder R A Systems Approach for Tumor Pharmacokinetics. PLoS One 2011, 6, e24696. [PubMed: 21935441]

35. Jain RK; Stylianopoulos T Delivering Nanomedicine to Solid Tumors. Nat. Rev. Clin. Oncol. 2010, 7, 653–664. [PubMed: 20838415]

36. Xu L; Kuang H; Xu C; Ma W; Wang L; Kotov NA Regiospecific plasmonic assemblies for in situ Raman spectroscopy in live cells. J. Am. Chem. Soc. 2012, 134 (3), 1699–1709. [PubMed: 22192084]

37. Shim BS; Zhu J; Jan E; Critchley K; Ho S; Podsiadlo P; Sun K; Kotov NA Multiparameter structural optimization of single-walled carbon nanotube composites: toward record strength, stiffness, and toughness. ACS Nano 2009, 3 (7), 1711–1722. [PubMed: 19591447]

38. Gheith MK; Pappas TC; Liopo AV; Sinani VA; Shim BS; Motamedi M Stimulation of Neural Cells by Lateral Currents in Conductive Layer-by-Layer Films of Single-Walled Carbon Nanotubes. Advanced Materials 2006, 18(22), 2975–2979.

39. Bhirde AA; Patel V; Gavard J; Zhang G; Sousa AA; Masedunskas A; Leapman RD; Weigert R; Gutkind JS; Rusling JF Targeted Killing of Cancer Cells in Vivo and in Vitro with EGF-Directed Carbon Nanotube-Based Drug Delivery. ACS Nano 2009, 3, 307–316. [PubMed: 19236065]

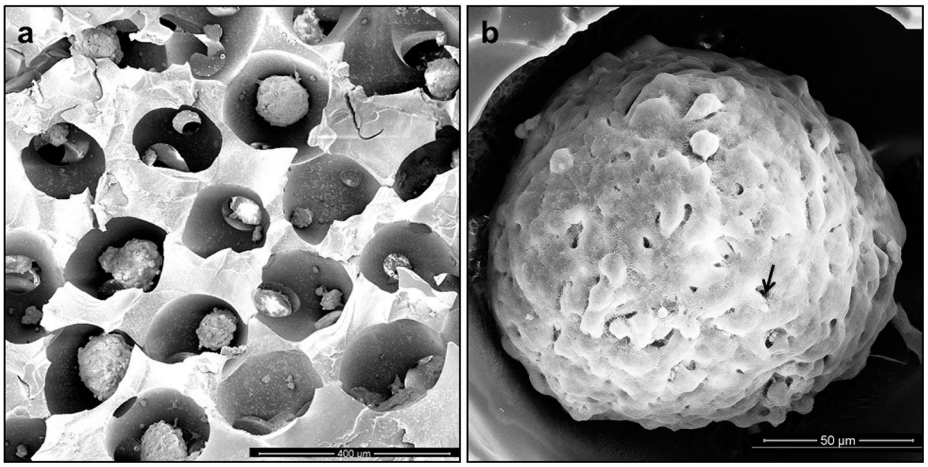

Figure 1.

SEM images of (a) dehydrated hydrogel ICC scaffolds cultured with cellular spheroids. Shape and pore diameter were shrunk during the dehydration process of SEM preparation. (b) SEM images of a mature spheroid in an ICC scaffold cultured for 5 days. Maturation of the spheroid is accompanied by formation of a layer of extracellular matrix on its surface, and individual cells become difficult to distinguish in the electron microscopy images. Scale bars: 400 μm (a) and 50 μm (b).

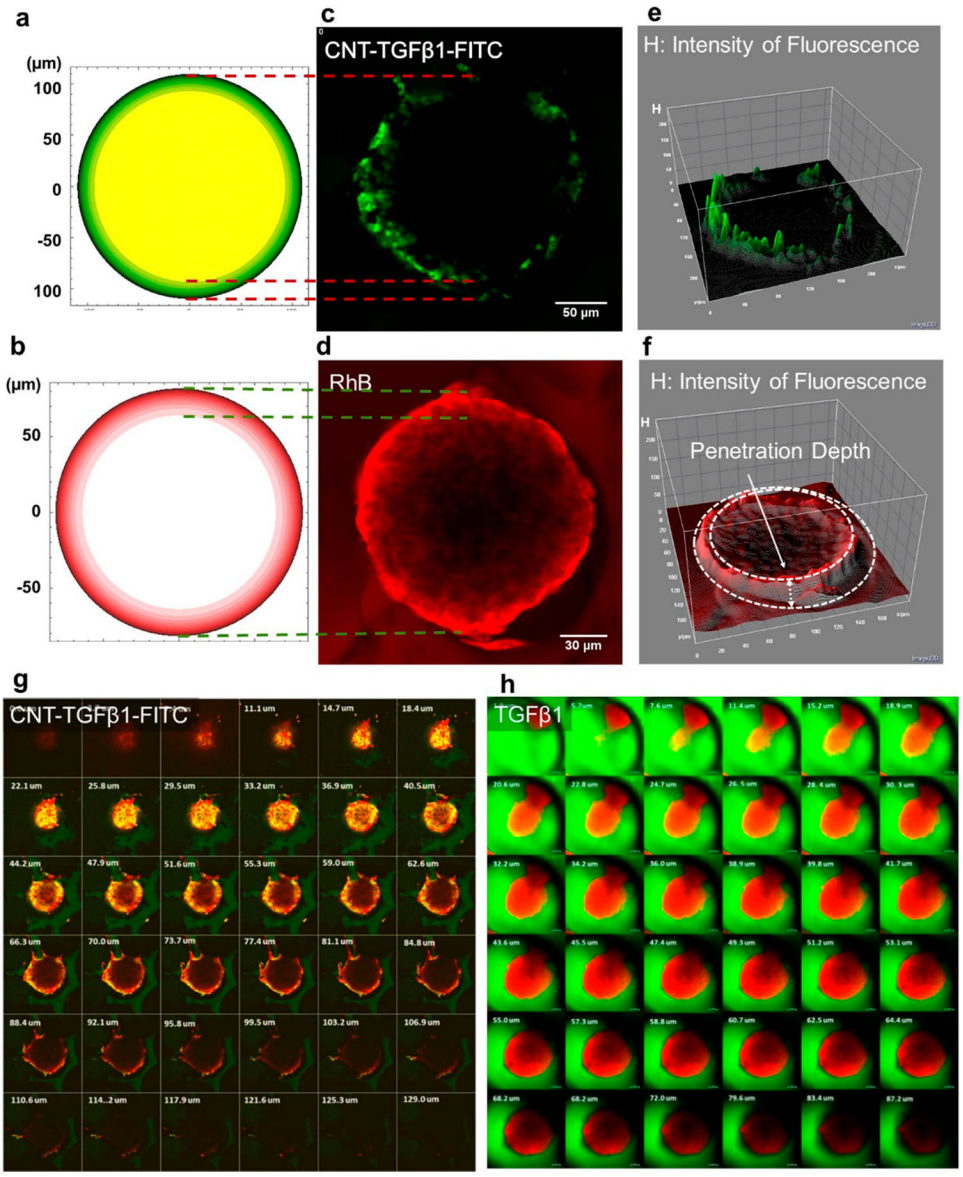

Figure 2.

Confocal imaging and modeling of diffusion profiles in HepG2 spheroids after 20 min exposure to fluorescent penetrants. (a) and (b) are calculated diffusion profile of CNT-TGFβ1-FITC and RhB, which compare to (c) and (d), permeation profiles of CNT-TGFβ1-FITC and RhB at central focal plane of the spheroid; (e) and (f) are the 3D surface plots of (c) and (d); H-axis represents the fluorescent intensity; the penetration depth is defined at the peak of fluorescent intensity. CNTs and TGFβ1 have green fluorescence in (c), (g) and (h); HepG2 cells in spheroids were stained red (CMTPX) before spheroid formation for images (g) and (h). Concentration of (d) free RhB (Red) is 1.1×10^{-4} mg/mL, and concentration of (h) free TGFβ1 is 3 μg/mL.

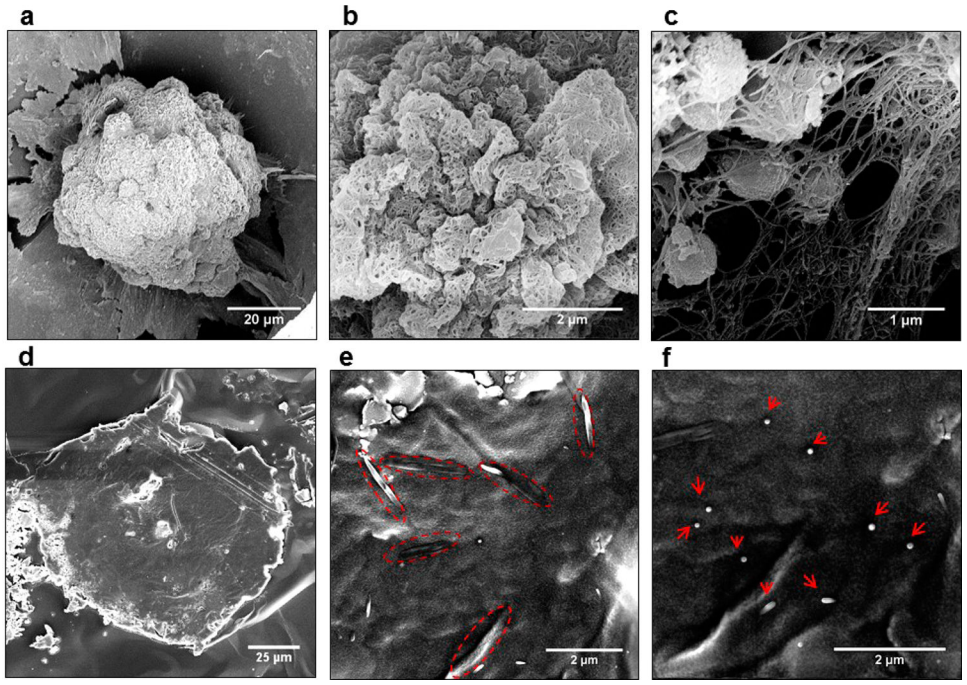

Figure 3.

SEM images of HepG2 spheroids after exposure to CNT-TGFβ-FITC for 20 min (a–c). The surface of the spheroid is at different magnification. CNTs in all the images could not be washed off without physical destruction of the tissue model, which indicated their penetration inside the cellular mass. Histological sections of HepG2 cell cultures (d) in ICC scaffolds with CNTs oriented predominantly in parallel (e) and perpendicular (f) alignment with the plane of sectioning.

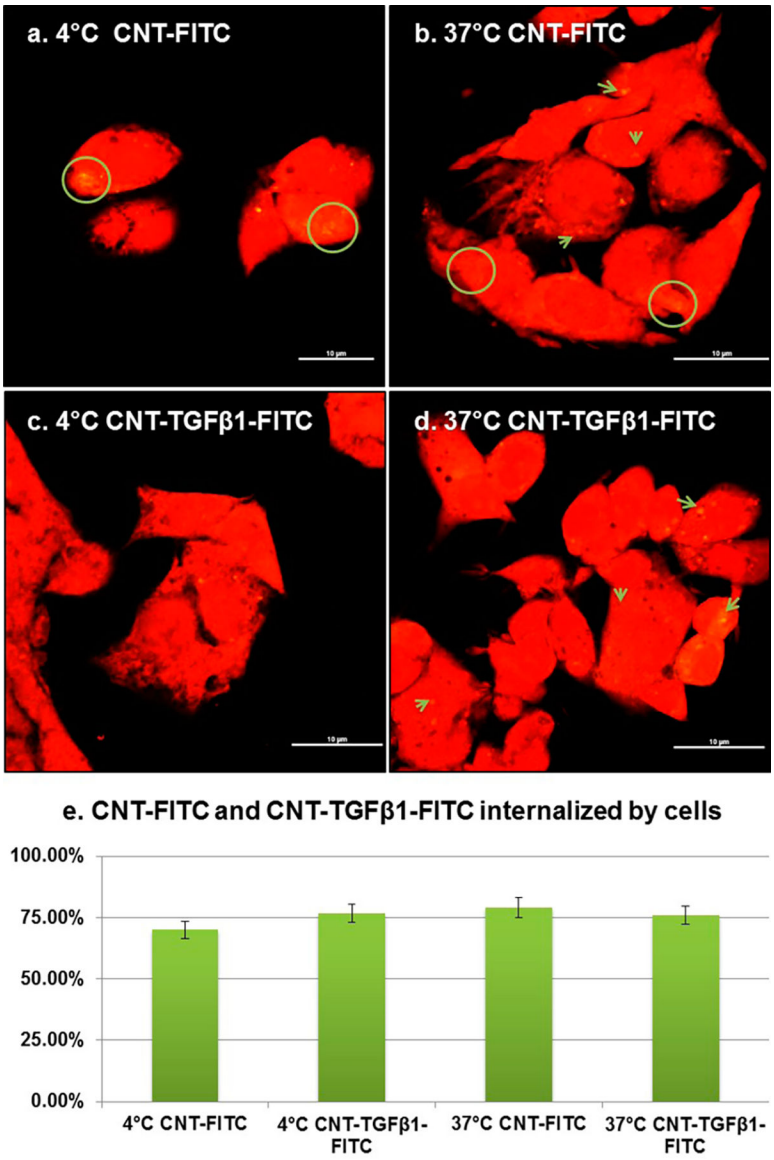

Figure 4.

Endocytotic internalization of CNT penetrants in 2D cell cultures. (a–d) Confocal microscopy images of HepG2 cells (red) after incubation for 1 h in serum-free medium with 0.5 mg/mL of CNT-FITC (a) and (b) or CNT-TGFβ1-FITC (c) and (d) at 4 and 37 °C. All scale bars are 10μm. (e) Quartification of CNT-FITC and CNT-TGFβ1-FITC internalized by cells at 4 and 37 °C. The percentage in (e) refers to flucrescent area fraction of CNTs to cells.

TABLE 1.

Experimental and Theoretical Stokes–Einstein Diffusion Coefficients for CNTs and Small Molecules

	apparent diffusion coefficient, D_a (m^2/s in PBS pH = 7.4)	diameter of HepG2 spheroid (μm)	ζ potential or molecular charge (mV) (in PBS pH = 7.4)	Stokes–Einstein diffusion coefficient, D (m^2/s in tissue)
CNT-TGFβ1-FITC	$(1.5 \pm 0.2) \times 10^{-13}$	141.9 ± 5.6	−8.4 ± 0.31	5.7×10^{-16}
CNT-FITC	$(0.9 \pm 0.3) \times 10^{-14}$	170.8 ± 4.5	−0.01 ± 0.001	5.7×10^{-16}
TGFβ1	$(2.5 \pm 0.3) \times 10^{-13}$	147.2 ± 5.0	−4.7 ± 0.02	5.7×10^{-15}
RhB	$(5.9 \pm 0.3) \times 10^{-13}$	139.7 ± 2.7	positive	1.8×10^{-14}
FITC	$(1.6 \pm 0.3) \times 10^{-14}$	136.4 ± 2.4	negative	4.1×10^{-14}